Monitoring Density Redistribution at the Excited State in a Dual Emitting Molecule: An Analysis Based on Real-Time Density Functional Theory and Density Descriptors

Feven-Alemu Korsaye, Fulvio Perrella, Alessio Petrone, Carlo Adamo, Nadia Rega, Ilaria Ciofini

Monitoring Density Redistribution at the Excited State in a Dual Emitting Molecule: an Analysis Based on Real Time Density Functional Theory and Density Descriptors

Feven-Alemu Korsaye[a†], Fulvio Perrella[b†], Alessio Petrone[c,b,d], Carlo Adamo[a], Nadia Rega[c,b,d], Ilaria Ciofini[a]**

nadia.rega@unina.it, ilaria.ciofini@chimieparistech.psl.eu

†These authors contributed equally.

a) *Chimie ParisTech, PSL University, CNRS, Institute of Chemistry for Life and Health Sciences, F-75005 Paris, France*
b) *Scuola Superiore Meridionale, Largo San Marcellino 10, I-80138, Napoli, Italia*
c) *Dipartimento di Scienze Chimiche, Università degli Studi di Napoli Federico II, via Cintia 21, I-80126 Napoli, Italia*
d) *Istituto Nazionale di Fisica Nucleare, Unità di Napoli, via Cintia 21, I-80126, Napoli, Italia*

Abstract

In this work we computed and analyzed, by the means of density based descriptors, the real time evolution of both the Locally Excited (LE) and Charge Transfer (CT) excited states for the planar and twisted conformations of the DMABN (the 4-(N,N- dimethylamino)benzonitrile molecule using Real Time-Time Dependent DFT and three different exchange correlation functionals (EXC) belonging to the same family (the PBE one).

Our results based on the analysis of density based descriptors show that the underlying EXC modifies the evolution in time of the density. In particular, comparing the frequency of density reorganization computed with the three functionals (PBE, PBE0 and LC-PBE) we found that the frequency of electronic interconversion of the individual determinants involved during the dynamics increases from PBE to PBE0 and to LC-PBE. This allows showing that there is a correlation between the delocalization of the electronic density and the frequency of reorganization. In particular, the greater the mean hole-electron distance during the dynamics the lower is the frequency of density reorganization.

1. Introduction

Density Functional Theory (DFT)[1] and Time-dependent DFT (TDDFT)[2] are quantum chemical methods extensively used to describe ground and excited states properties and reactivity of molecular systems. These methods are indeed providing generally accurate results at a computational cost that makes them applicable and reliable also for the description of medium to large size molecular systems[3].

The success of DFT and TDDFT is clearly linked to the development of increasingly accurate approximate exchange-correlation functionals (XC) that have been the subject of intensive research and benchmarking in the last decades. Several studies have also clearly pointed out some impacts of the use of approximate XC and their consequences on the reliability of the computed properties. For what concerns the description of excited states by the means of methods rooted on TDDFT, it is nowadays well established that these methods may fail to reproduce the correct 1/R asymptotic behavior (with R the distance between the electron and the hole charge distribution) due to the approximated nature of the exchange and correlation functional used to express the total energy of the system[4,5,6,7,8,9,10,11]. As a consequence, the description of excited state with long-range Charge Transfer (CT) character or, more generally, of localized charge separated states[12,13,14,15] may result inaccurate depending on the XC used. In particular, previous linear response (LR-)TDDFT studies have shown how CT excited states energies are typically underestimated, using Local-Density Approximation (LDA)[16,17] or Generalized Gradient Approximation (GGA)[18,19,20] functionals while the functionals restoring partially or completely the correct 1/R behavior incorporating a fraction or full exact exchange (such as Global Hybrids (GH)[21,22] or, Range Separated Hybrids (RSH)[23,24] functionals) mitigate this error.

In some cases, this error may lead to the prediction of unphysical low lying -dark- states, commonly referred to as ghost states, or unphysical states, which may induce the derivation of a misleading picture of the photophysics of the molecular systems considered[4-11]. Ghost states have been indeed identified in the description of excited states conducted using LR-TDDFT within the Casida's formalism[25] which is the most employed formulation of TDDFT enabling the calculation of properties directly related to the optical spectra of molecules.[26] More scarce are, on the other hand, the works making use of Real-time TDDFT (RT-TDDFT)[27,28,29,30], where the application of the perturbation is followed by the propagation of the electron density via numerical integration,

for which a deep analysis of the electronic density reorganization and its evolution in time[31,32] was performed together with an identification of possible ghost states.[33]

In this context, various indexes have indeed been developed both to describe from a quantitative point of view the CT[34,35,36,37, 38,39,40,41,42] and to estimate the reliability of the predicted excited states (ES) energies[43,44,45]. Some of these indexes, based on the analysis of the electron and hole charge distributions, were developed by some of us in the last years. These indexes were used in the framework of LR TDDFT both to quantify the hole-electron distance (that is the charge transfer extent) by the means of the D_{CT} family[34-36] and/or to diagnostic possible artifacts in calculations, using the so-called M_{AC} index[44,45] which provides a lower bound of the transition energies and thus allows to spot unphysically low lying states. Only in a recent work, the same tools were generalized to the RT-TDDFT formalism and used to describe and diagnostic on the fly the electronic density evolution upon real time propagation for a family of simple rod-like push-pull molecules.[33]

This analysis confirmed that attoseconds electron dynamic simulations can be affected by the same artifacts known for LR-TDDFT approaches. Nonetheless, our analysis was performed focusing exclusively on the lowest lying excited state and considering only a local exchange and correlation functional (namely SVWN) for which the artifacts stemming from the approximate nature of the exchange and correlation energy functional (EXC) are expected to be more evident.

To understand how these index may be of further relevance for the interpretation of excited states evolution in more complex systems described at RT-TDDFT level, in the present work we have considered a simple molecule, largely theoretically studied, displaying dual emission in polar solvents, that is DMABN (the 4-(N,N- dimethylamino)benzonitrile, schematically represented in Figure 1)[46,47,48,49,50,51,52.] This molecule shows two bright emitting states normally classified as a Locally Excited (LE) one and a CT one. Depending on the relative orientation of the dimethylamino group with respect to the benzonitrile plane (ruled by the θ twisting angle, Figure 1) the relative stability of the two states changes. In particular, while the emitting LE excited state has been linked to the molecule in planar structure ($\theta = 0^o$), different molecular geometries have been proposed for the emitting CT state[53,54,55,] among which the twisted geometry is considered the most plausible.[56,57] In this contribution, we have computed for both planar and twisted conformations the real time evolution in gas phase of the density of both the LE and CT excited states using different functionals by the means of the RT-TDDFT approach and analyze it by the

means of different density based descriptors to see if and how the underlying EXC modify the evolution in time of the density.

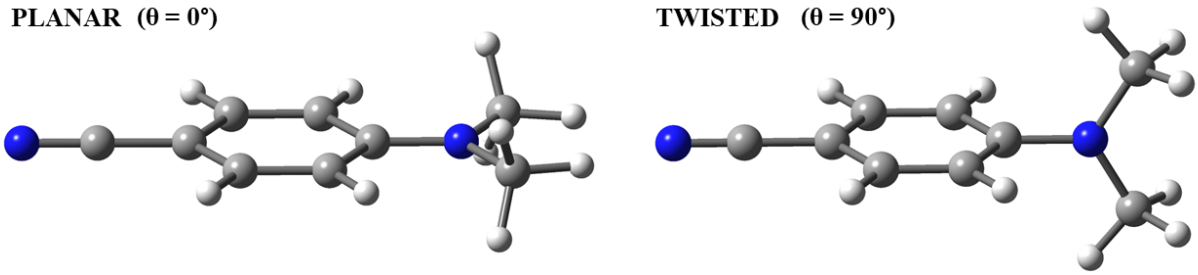

Figure 1. The planar and twisted geometries of the DMABN molecule which depend on the value of the angle θ (formed by the plane of the dimethylamino group and the benzonitrile plane).

2. Methods

Density based descriptors In order to determine the spatial extent associated to an electronic excitation in the LR regime and the extent of density rearrangement during electron dynamics, we made use of the D_{CT} (distance of the charge transfer) original index[34]. The latter provides a measure of the hole-electron distance using only the densities of the ground state and the excited state of interest. The procedure can be synthesized in four simple steps:

I) the electron density variation is computed as the difference between the ground and excited state densities: $\Delta\rho(\boldsymbol{r}) = \rho_{ES}(\boldsymbol{r}) - \rho_{GS}(\boldsymbol{r})$

II) two functions are defined representing the regions in space around the molecule characterized by a density increment ($\rho_+(r)$) and deletion ($\rho_-(\mathrm{r})$) after excitation

III) the barycenters of the density increment ($\boldsymbol{R}_+$) and depletion ($\boldsymbol{R}_-$) regions are computed

IV) the distance of the charge transfer is obtained as the distance between the two barycenters: $D_{CT} = |\boldsymbol{R}_+ - \boldsymbol{R}_-|$.

The D_{CT} index provides a qualitative measure of the distance of the charge transfer (referred to here as D_{CT} values), allowing a given excited state to be easily classed as a charge transfer or locally excited state. For a locally excited state we expected a D_{CT} value very close to zero while a partial CT character will correspond to D_{CT} around 2Å or larger. Additionally, one can define two charge centroids associated to the density increment (C_+) and depletion (C_-) regions, which allows to obtain a simple visual representation of the spatial extent of the charge transfer. Different

formulations of the D_{CT} index allowing its generalization to symmetric systems were also further developed. [35,36]

In the electron dynamics domain, the descriptor is computed directly on selected snapshots along the RT simulation trajectory as the difference in density between the actual propagated density and the initial ground state density. In this case the computed D_{CT} values along the RT trajectory will reflect the evolution of the electron density reorganization and can be used as tool to quantify the extent of the density rearrangement during the simulation.

The D_{CT} index can also be used to define the M_{AC} (Mulliken averaged configuration) index,[44,45] which was developed by some of us with the aim of understanding the reliability of different XC in describing charge transfer processes. The formulation of the M_{AC} index stems from a formula originally proposed by Mulliken, which allows to estimate the lower bound of a net one-electron intermolecular charge transfer (ω_{CT}) between a donor (D) and an acceptor (A) as:

$$\omega_{CT} = IP_D - EA_A - \frac{1}{R}, \quad (1)$$

where IP_D, EA_A and R are the ionization potential of the donor, the electron affinity of the acceptor and the geometrical distance between the donor and the acceptor groups, respectively. Using a Koopman-type approach, the M_{AC} index is computed by replacing IP_D and EA_A with the weighted average of the energies of the initial occupied (ϵ_i) and final virtual (ϵ_a) Kohn-Sham orbitals, respectively:

$$M_{AC} = \frac{\sum_{ia} [{C_{ia}}^2 (\epsilon_a^{DFT-HF} - \epsilon_i^{DFT-HF})]}{\sum_{ia} {C_{ia}}^2} - \frac{1}{D_{CT}}, \quad (2)$$

where the weights C_{ia} are the CI coefficients obtained as solution of TDDFT equations. Of note, deexcitation amplitudes are negligeable in our case allowing the direct use of the CI coefficients. In eq 2, the energies of the orbitals obtained using DFT theory are corrected with a single SCF cycle using Hartree-Fock theory (now referred as ϵ^{DFT-HF}) to correct their possible underestimation due to the approximated nature of the exchange and correlation functional. In addition, the geometrical distance R between the donor and acceptor is here replaced by the hole-electron distance computed with the D_{CT} index. The M_{AC} computed in that way will then represent the lower bound to the excitation energy. Therefore, by comparing this energy value with the transition energy computed at TDDFT level of theory, one can determine whether the predicted energy with a given XC is actually underestimated (referred to as *unphysical state*) or not (referred to as *real state*):

$$E^{TD-DFT} > M_{AC} \rightarrow \text{ Real State,} \quad (3)$$

$$E^{TD-DFT} < M_{AC} \rightarrow \text{ Unphysical State.} \quad (4)$$

Recently[33], we have adapted this index for its use in the real-time TDDFT domain. This is done by expressing the density reorganization during the simulation as a function of the population of the ground state occupied and virtual molecular orbitals (n_{occ} and n_{vir}) along the electron dynamics. As consequence, the MAC index will be computed at every selected timestep during the simulation, leading to a set of $M_{AC}^{RT}(t_j)$ energy values representing the lower bound to the energy associated to the different density distributions experienced during the electronic dynamics:

$$M_{AC}^{RT}(t_j) = \frac{\sum_{vir}[n_{vir}(t_j)\epsilon_{vir}{}^{DFT-HF}] - \sum_{occ}[n_{occ}(t_j)\epsilon_{occ}{}^{DFT-HF}]}{\sum_{vir} n_{vir}(t_j) + \sum_{occ} n_{occ}(t_j)} - \frac{1}{D_{CT}(t_j)}. \quad (5)$$

Finally, by comparing the set of energy values obtained from eq 5 with the total energy of the system during the simulation, one can identify those unphysical density distributions whose energies are incorrectly predicted by using a given exchange and correlation functional.

Computational details The two geometries of the DMABN molecule have been optimized at the ground state in the gas phase using the PBE0 functional[21] and the 6-31+G(d) basis set. The latter, together with the optimized structures, is reported in the SI. The vertical excitation energies are obtained using LR-TDDFT with 6-31+G(d) basis set and PBE,[18] PBE0[21] and LC-PBE[24] functionals. The same level of theory has been used for the RT-TDDFT dynamics. The excited state densities of interest are prepared by promoting an electron from a selected occupied molecular orbital to one that is unoccupied in the ground state (Koopman excitation) according to the electronic transition of interest between the singlet ground state minimum (S_0) and the nth singlet excited state (S_n), whose main orbital contributions are resolved using preliminary frequency domain LR-TDDFT calculations. The Koopman excitation step creates a non-stationary electron density, representing a coherent superposition of the ground and the excited state(s) of interest.[58,59,60,61,62,63,64] The densities prepared in this way were then propagated according to the non-linear Liouville-von Neumann equation[65]

$$i\hbar \frac{\partial \boldsymbol{P}(t)}{\partial t} = \left[\boldsymbol{F}\left(\boldsymbol{P}(t)\right), \boldsymbol{P}(t)\right] \quad (6)$$

where $\boldsymbol{P}$ is the one-particle reduced density matrix and $\boldsymbol{F}$ is the Fock (Kohn-Sham within DFT) matrix in an orthonormal basis. Given an initial time t_0, $\boldsymbol{P}(t)$ can be formally propagated in time through the Magnus expansion of the time-domain propagator $\boldsymbol{U}(t, t_0)$:

$$\boldsymbol{P}(t) = \boldsymbol{U}(t, t_0)\boldsymbol{P}(t_0)\boldsymbol{U}^{\dagger}(t, t_0) \quad \boldsymbol{U}(t, t_0) = \exp\left(\boldsymbol{\Omega}(t, t_0)\right) \quad (7)$$

where $\boldsymbol{\Omega}(t, t_0)$ is a series expansion which has to be truncated in practice. In particular, the modified midpoint unitary transformation[66] (MMUT) was employed to integrate Eq. (6) in time. MMUT is an explicit multistep symplectic integration scheme, with an error proportional to Δt^2:

$$\boldsymbol{P}(t_{k+1}) = \boldsymbol{U}(t_k)\boldsymbol{P}(t_{k-1})\boldsymbol{U}^{\dagger}(t_k) \quad \boldsymbol{U}(t_k) = \exp\left(-\frac{2i\Delta t}{\hbar}\boldsymbol{F}(\boldsymbol{P}(t_k))\right) \quad (8)$$

where t_k is the current time step.

Since we are not allowing the nuclei to move (fixed nuclei approximation, by starting from a minimum geometry), this procedure can be used as a reasonable approximation of a vertical excitation in the Franck-Condon region in the ultrafast regime (~ 50 fs). In such a short time, indeed, it could be assumed that the effect of nuclear vibrations is still limited. Therefore, the "fixed nuclei" approximation implied in these purely electronic dynamics is reasonable.

DMABN RT-TDDFT simulations were carried out with a propagation time step of 0.25as, for a total simulation time of 20fs. Such time step ensured an energy drift within 10^{-6}Ha. Density snapshots and orbital populations were extracted every 0.1fs. All LR calculations and RT simulations were performed using Gaussian16 and the Gaussian development versions[67,68], respectively.

3. Results & Discussion

LR TDDFT calculations Preliminary to RT-TDDFT calculations, vertical LR-TDDFT computations have been performed on the stable planar and twisted conformers. The outcomes of these calculations are summarized in Table 1 and will be used as reference in the discussion of RT-TDDFT results. In line with previous literature reports[46,47,48], the data obtained at PBE, PBE0

and LC-PBE level show the presence of two states, one displaying a larger CT character (labelled as CT), as easily quantified by the D_{CT} value, and a more localized one (labelled LE). Upon rotation of the donor -dimethylamino- group the two states invert: for a planar conformation the LE is the most stable, while for a twisted CT becomes the lowest in energy. In agreement with the analysis of Tozer and collaborators[46], the computed D_{CT} values as well as the corresponding hole and electron centroids of charge (reported in Figure 2) show how, at the twisted conformation, both states actually present a sizable CT character and are thus expected to be affected by errors depending on the EXC applied. Indeed, the computed M_{AC} energies (Table 1) confirm that PBE is underestimating the energy of both CT and LE states at the twisted conformation while the hybrid functionals (PBE0 and LC-PBE) are correctly predicting LE energy and ameliorating (PBE0) or correcting (LC-PBE) the energy prediction for the CT state.

	PBE			PBE0			LC-PBE		
	E (eV)	M_{AC}(eV)	D_{CT} (Å)	E (eV)	M_{AC}(eV)	D_{CT} (Å)	E (eV)	M_{AC}(eV)	D_{CT} (Å)
Planar LE	4.04	-	0.98	4.54	-	0.87	5.00	-	0.67
Planar CT	4.34	1.77	1.87	4.75	1.30	1.81	5.14	-	1.48
Twisted LE	3.00	3.37	1.86	4.12	3.64	1.91	5.78	3.02	1.75
Twisted CT	2.34	4.50	2.31	3.36	4.52	2.30	4.60	4.59	1.95

Table 1. Transition energies (eV), D_{CT} (Å) and M_{AC} energy values (eV) of the CT and LE states in the planar and twisted geometries using PBE, PBE0 and LC-PBE functional. The excitation energies predicted to be underestimated by the M_{AC} index are marked in red.

As described in the Computational Details, in order to simulate the CT and LE states in RT simulations, single determinant contributions of LR TDDFT states were analyzed. Table 2 collects for both geometries the main individual determinants contributing to the two excited states along with their weight in percentage terms. The orbitals involved are depicted in Figure 2. In agreement with previous reports, the only determinant that contributes significantly (>80%) to the CT states involves an electron transfer from the HOMO → LUMO, while the LE states are mainly the result of a HOMO → LUMO+1 excitation (LUMO+2 in the case of the LC-PBE functional). Therefore, starting density for the RT TDDFT simulation was obtained by populating the single determinant |CT1> and |LE1>, constructed promoting an electron from the HOMO to LUMO and from the HOMO to LUMO+1 orbital (LUMO+2 for LC-PBE), respectively, for the CT and LE states simulation. We should nonetheless note that in some cases a small but sizable contribution of a second single determinant (such as the |LE2> and |CT2> in case of the planar conformations) is present.

PLANAR			
	PBE	PBE0	LC-PBE
LE	$\|LE1\rangle$ HOMO →LUMO+1 92% $\|LE2\rangle$ HOMO-1→LUMO 0.05%	$\|LE1\rangle$ HOMO →LUMO+1 90% $\|LE2\rangle$ HOMO-1→LUMO 1%	$\|LE1\rangle$ HOMO →LUMO+2 82% $\|LE2\rangle$ HOMO-1→LUMO 0.14%
CT	$\|CT1\rangle$ HOMO →LUMO 92% $\|CT2\rangle$ HOMO-1→LUMO+1 0.03%	$\|CT1\rangle$ HOMO →LUMO 95% $\|CT2\rangle$ HOMO-1→LUMO+1 0.03%	$\|CT1\rangle$ HOMO →LUMO 92% $\|CT2\rangle$ HOMO-1→LUMO+2 0.03%
TWISTED			
LE	$\|LE1\rangle$ HOMO -> LUMO+1 100%	$\|LE1\rangle$ HOMO → LUMO+1 100%	$\|LE1\rangle$ HOMO → LUMO+1 95%
CT	$\|CT1\rangle$ HOMO → LUMO 100%	$\|CT1\rangle$ HOMO → LUMO 98%	$\|CT1\rangle$ HOMO → LUMO 87% $\|CT2\rangle$ HOMO → LUMO+24 0.04%

Table 2. Single determinants predominantly contributing to the CT and LE states, with their weight in percentage terms, in the planar and twisted geometries using PBE, PBE0 and LC-PBE functionals.

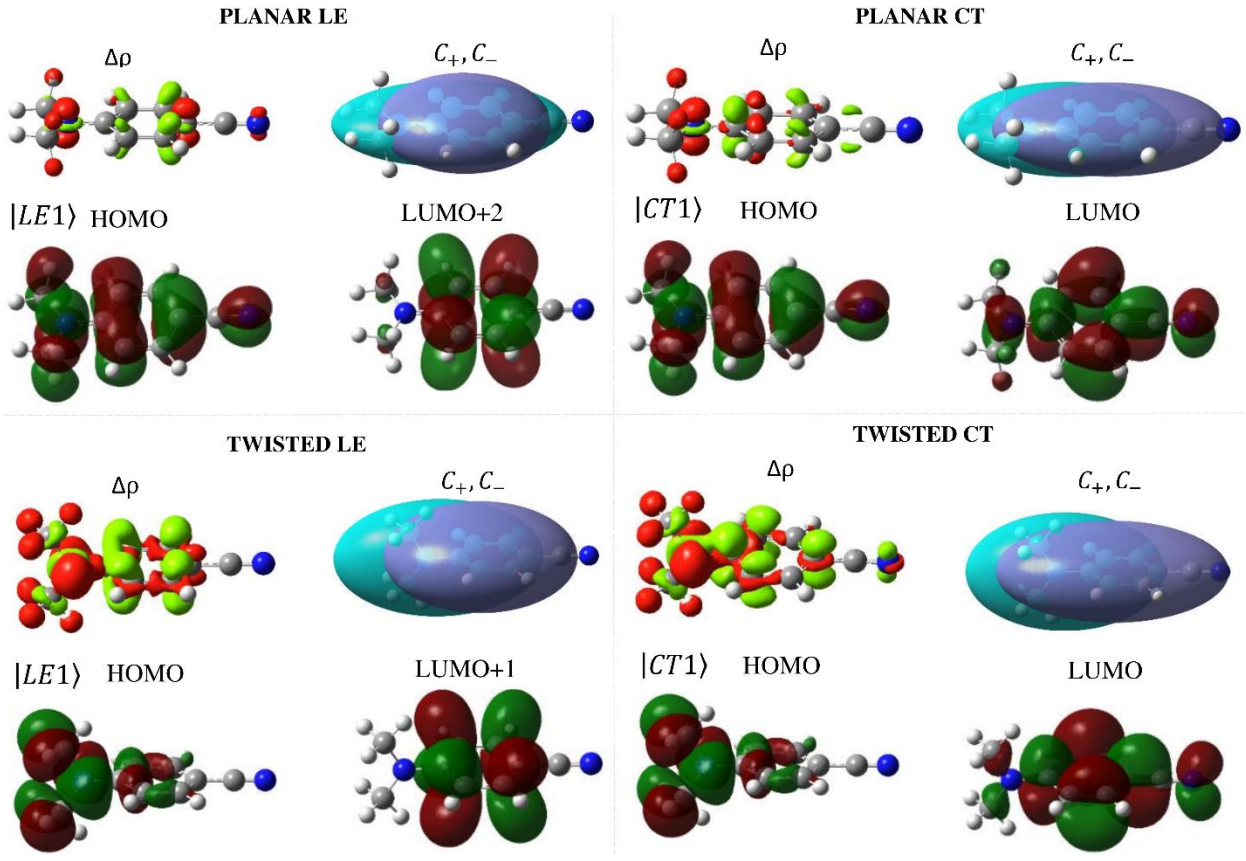

Figure 2. Molecular orbitals (MOs) mainly involved, density variation upon excitation (Δρ) and centroids of charges (C_+, C_-) of the CT and LE states in the planar and twisted geometries with LC-PBE functional. The isovalue of the MOs and Δρ are 0.02 and 0.004, respectively. The red and green colors of the density variation represent the density depletion and increment after excitation, respectively.

RT TDDFT simulations For each functional four RT simulations were performed starting from the above mentioned single determinants (|CT1> and |LE1> representing the CT and LE states, respectively) at planar and twisted structures. For simplicity from here on we will refer to them as *CT* and *LE* although these are clearly not corresponding to the real CT and LE pure states. In Figure 3 are reported the D_{CT} values calculated at LC-PBE level along the four trajectories (refer to SI for corresponding PBE and PBE0 plots) which provide an on-the-fly measure of the hole-electron separation during the dynamics. For each simulation, the average of the D_{CT}s value computed during dynamics (labelled as mean RT) and the corresponding LR value (labelled as LR) are also reported in Table 3. Regardless of the functional used, the largest difference between the mean RT and LR D_{CT} value is computed for the *CT* at the planar geometry. This difference indicates a significant reorganization of the electronic configuration with respect to the starting density as a consequence of hole-electron redistribution. In particular, the lower RT mean D_{CT} value is explained by the ultrafast density oscillation between donor and acceptor moieties characterizing *CT* charge dynamics. Furthermore, the difference between mean RT and LR values increase going from LC-PBE to PBE0 to PBE. Similarly, the higher amplitude of the D_{CT} oscillations is observed for the *CT* dynamics independently of the functional, while the other three dynamics (i.e. planar *LE*, twisted *LE* and *CT*) show a D_{CT} that doesn't change significantly, meaning that the charge densities fluctuate little around the mean value.

Following eq 5, the corresponding M_{AC} values were next computed along the dynamics and compared with corresponding RT energies thus allowing to identify the density distribution along the simulation corresponding to non-physical states. The latter are identified in red in Figure 3 and in Figure S2-3. Regardless of the functional used, no dynamics shows a significant presence of non-nonphysical states. More specifically, in the case of LC-PBE (Figure 3) non-physical states are explored only in the case of the twisted *CT* simulation and in the case of the twisted LE only the starting point is displaying a density distribution corresponding to a non-physical state. We should nonetheless point out that the RT energy is much larger than the corresponding LR energy thus explaining why, also in the case of the PBE0 and PBE functionals most of the charge distribution explored are considered as corresponding to a physical state. In these regards, it has to be remarked that the initial density of RT dynamics corresponds to a photogenerated electron and hole. Such density resembles the most the excited state of interest, but it corresponds to a nonequilibrium superposition of eigen-states.[29] Therefore, the initial RT energy (then conserved

along all the simulation) results always higher than that of the corresponding (LR resolved) excited eigenstate.

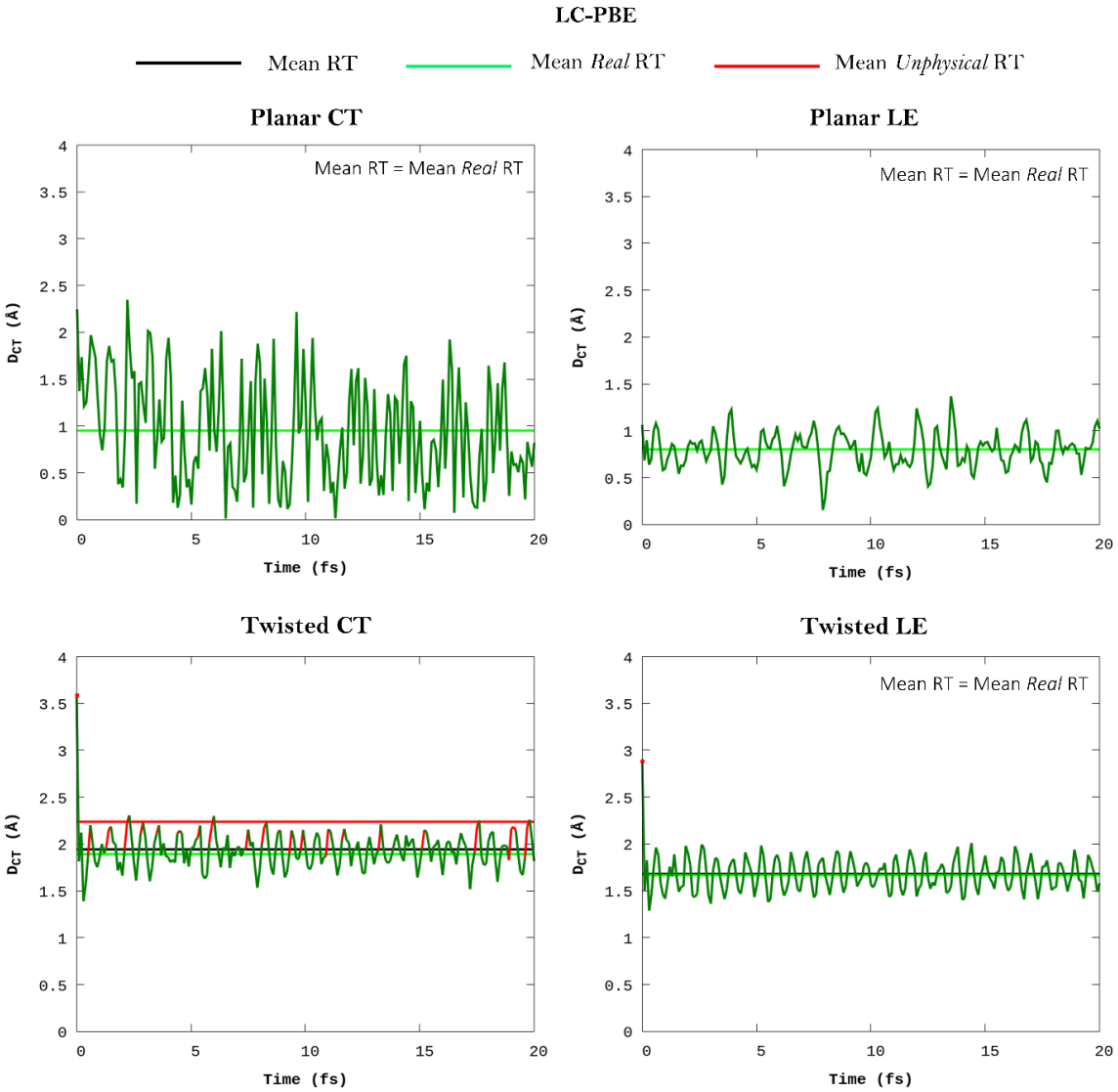

Figure 3. D_{CT} values (Å) of *CT* and *LE* simulations in the planar and twisted geometry obtained with LC-PBE functional. The average of all D_{CT} values in RT, the average D_{CT} value obtained from the correct density distributions, and the average D_{CT} value obtained from the non-physical density distributions are represented as black, green, and red lines, respectively. The average of all D_{CT} values and the average D_{CT} value obtained from the correct density distributions are the same for the simulations of *CT* and *LE* at planar geometry and *LE* at twisted geometry.

	PBE				PBE0				LC-PBE			
	LR	RT^{MEAN}	Δ	A	LR	RT^{MEAN}	Δ	A	LR	RT^{MEAN}	Δ	A
PLANAR												
LE	0.98	0.55	0.44	1.28	0.87	0.71	0.18	0.90	0.67	0.80	0.19	1.21
CT	1.87	0.94	0.50	2.10	1.81	1.07	0.41	2.71	1.48	0.95	0.36	2.34
TWISTED												
LE	1.86	1.57	0.16	1.57	1.91	1.72	0.10	0.81	1.75	1.68	0.04	0.72
CT	2.31	1.82	0.21	1.01	2.30	2.03	0.12	0.91	1.95	1.94	0.01	0.91

Table 3. D_{CT} values (Å) obtained from LR calculations, mean D_{CT} values of *CT* and *LE* simulations, and relative difference between LR and mean RT values (Δ) and oscillation amplitude (A) for the planar and twisted geometry using PBE, PBE0 and LC-PBE functional. The value of A is calculated as the difference between the maximum and minimum D_{CT} values right after the first 0.1 fs of the simulation.

Let's now focus on how the planar *CT* density evolves over time. For this purpose, we consider how the population of molecular orbitals evolves during the dynamics. To this end we have set a threshold for population change 0.1 electron and consider all MOs with changes above this threshold. Regardless of the functional, the orbitals involved are those of the single determinants |CT1> and |CT2> that actually mostly contribute to the CT state as reported in Table 2. Specifically, the dynamics is initiated by populating only the $|CT1>_{alpha}$ determinant, that is removing an alpha electron from the HOMO and populating the alpha LUMO. Once the dynamics is initiated, the system reorganizes as a result of the coulombic interaction between the electron and the generated hole, and the only other orbitals that become significantly involved in this hole-electron delocalization are the beta orbitals of the simple |CT1> determinant and the alpha and beta of the |CT2> determinant. Figure 4 shows how this behavior is qualitatively the same for all functionals analyzed.

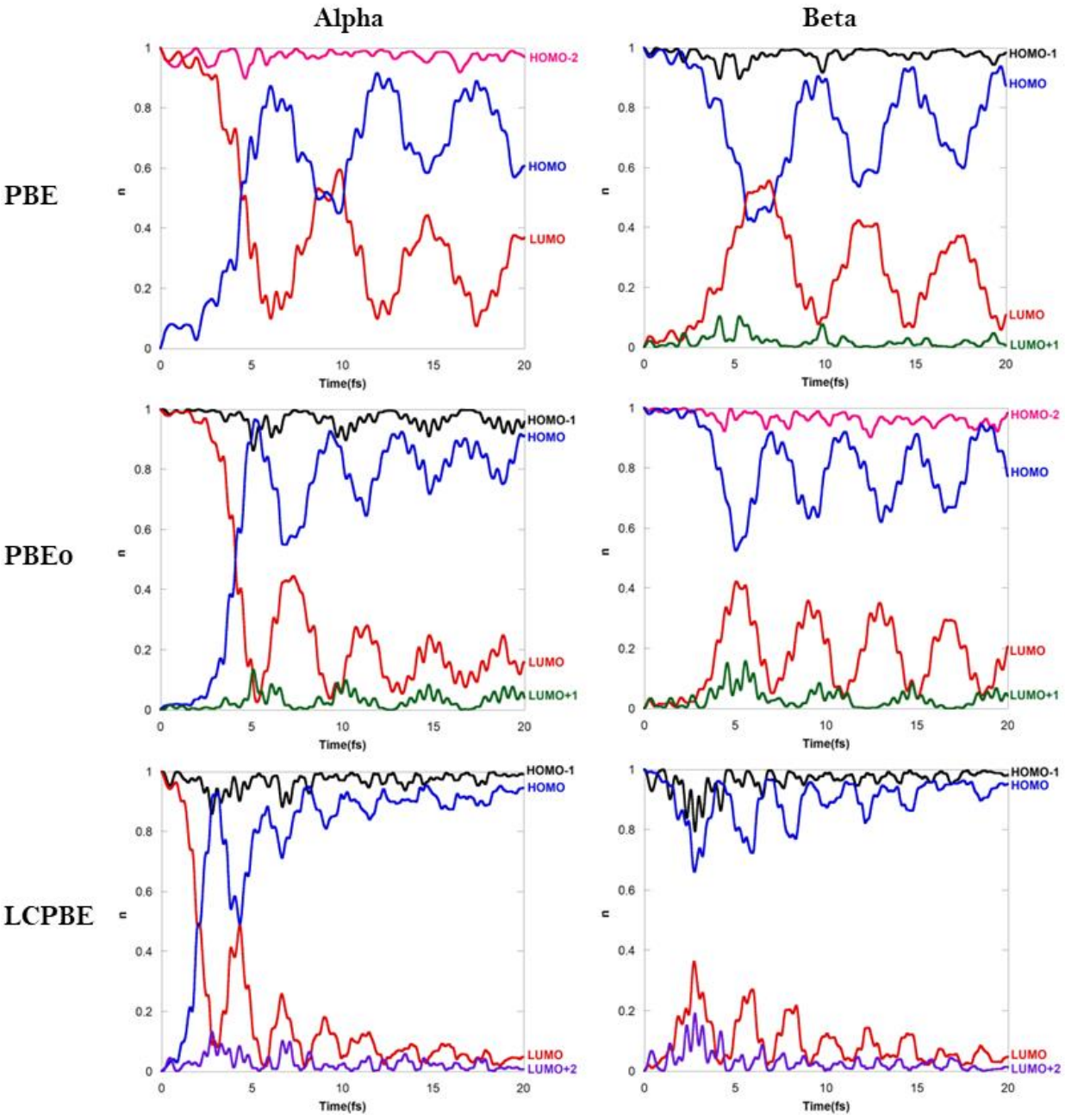

Figure 4. Population of alpha and beta MOs involved in the *CT* dynamics at planar geometry using PBE, PBE0 and LC-PBE functional. The threshold used for the population variation is 0.1 fraction of electron.

In the case of the LC-PBE functional we performed a more quantitative analysis of the orbital contribution, as reported in Figure 5. In this figure, the absolute value of the population changes with respect to ground state of the individual occupied (and virtual) molecular orbitals is plotted in percentage terms with respect to the overall population change over all occupied (and virtual)

orbitals. It can be seen that, after an initial reorganization time taking place in about 5fs, the orbitals of the simple determinant |CT1> are the ones that determine 80 % of the electronic reorganization, 5 % are those of the simple determinant |CT2>, while the remaining 15 % involve 28 molecular orbitals that, however, undergo a population change of less than 0.1 electron each. This leads to the exclusion of significant involvement of other single determinants than |CT1> and |CT2> and thus the mixing of outer electronic states.

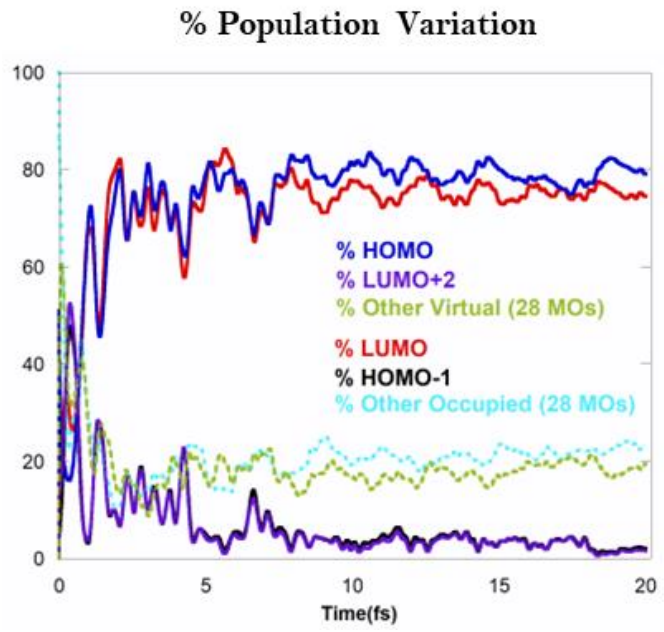

Figure 5. The population variation percentage of the most involved MOs for the *CT* simulation at planar geometry using LC-PBE functional. All the orbitals with a population variation ≤ 0.1 fraction of electron are included in *Other Virtual* and *Other Occupied*.

Moreover, this density reorganization, in addition to significantly affecting only the two single determinants that constitute the CT state itself, occurs through a population/depopulation which takes place within the same determinant. This can be visualized by the analysis of the Fourier transform of the population oscillations of the orbitals reported in Figure 6 for the LC-PBE functional (and in SI for the PBE and PBE0 simulation). It can be seen that the oscillation frequency and amplitude are the same for orbitals belonging to the same determinant, indicating a density reorganization that results from electronic interconversion within the same single determinant. In other words, what happens during the RT dynamics is an oscillation of the contribution of the individual single determinants that contribute to the CT state.

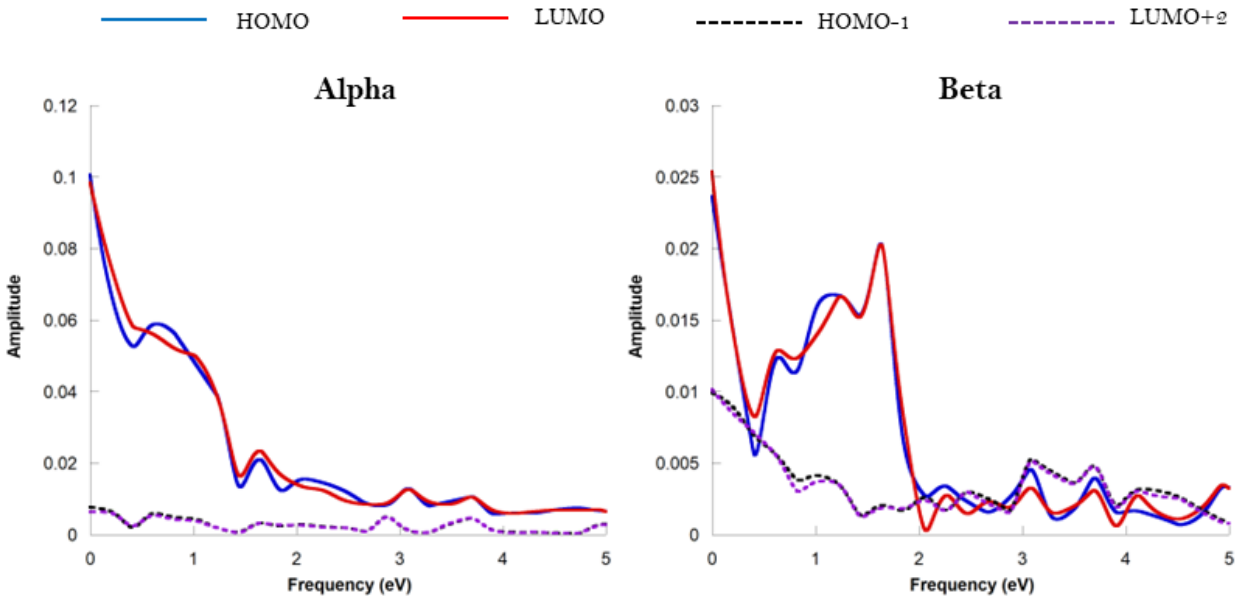

Figure 6. Fourier transform of the population of the mainly involved molecular orbitals in the *CT* dynamics in planar geometry using the LC-PBE functional.

Further analysis of Figure 4 allows to show how, the electron initially promoted in the LUMO alpha orbital progressively populates the HOMO alpha orbital, while the other occupied (HOMO beta, HOMO-1 beta) and virtual (LUMO beta, LUMO+2 beta) orbitals undergo a population/depopulation that occurs at a constant frequency but with a decreasing amplitude. This indicates a progressively important involvement of the ground state determinant |GS>. A progressive population of the ground state thus occurs, but since there is no energy dissipation the system maintains a stable energy by populating high-energy virtual orbitals and oscillating with constant frequency around the ground state density.

The involvement of the ground state determinant is what determines the dynamics in the case of *CT* at planar geometry. On the other hand, in the case of *LE* at planar geometry and *CT* and *LE* at twisted geometry ground and excited states are characterized by a different symmetry. This results in the fact that mixing with the ground state has a lower probability. As a consequence of this, the single determinant populated at the beginning of the simulation will be the only one involved during the dynamics of these states, resulting in a nonsignificant density swing around the starting density, as shown by the D_{CT} analysis in Figure 3.

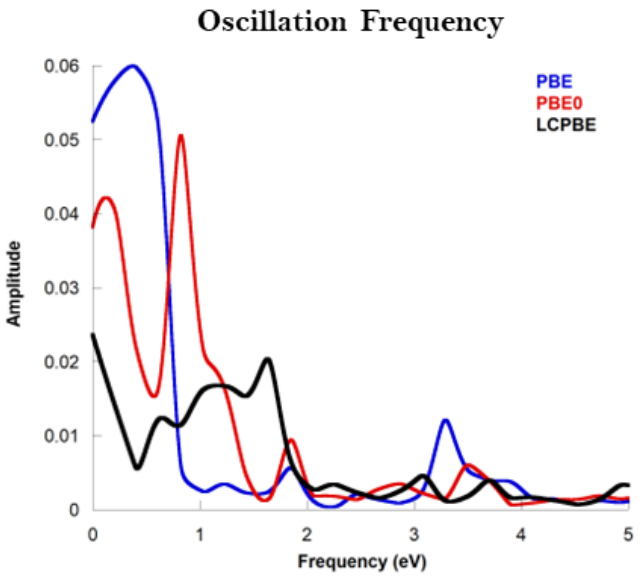

Figure 7. Fourier transform of the HOMO-beta orbital population in the *CT* dynamics at planar geometry using PBE, PBE0 and LC-PBE functionals.

Finally, in order to highlight the differences between the three functionals, we compare the frequency of density reorganization computed with the three functionals by analyzing the Fourier transform of the change in populations of the $HOMO_{beta}$ orbital obtained with PBE, PBE0 and LC-PBE, shown in Figure 7. Since from Figure 6 it can be seen that the frequency of oscillation $HOMO_{alpha}$=$LUMO_{alpha}$=$HOMO_{beta}$=$LUMO_{beta}$, the HOMO beta orbital is chosen here only for convenience. It is noticed that the frequency of electronic interconversion of the individual determinants involved during the dynamics increases from PBE to PBE0 and to LC-PBE. This result is related to the percentage of Hartree Fock exchange present in the functionals (0% PBE, 25% PBE0, 100% long range LC-PBE). In fact, the lower the HF exchange, the greater the delocalization of the electronic density, thus a greater distance between the barycenter of the positive and negative charges. This trend is indeed observed in the D_{CT} values calculated in both the LR and RT approaches (Table 3), which show charge transfer distances that decrease as the percentage of HF exchange used in the functional increases. Consequently, since the electronic reorganization of the system is a result of electrostatic hole-electron interaction, a greater hole-electron distance (PBE>PBE0/LC-PBE) results in a lower frequency of density reorganization (PBE<PBE0/LC-PBE).

4. Conclusions

The analysis performed, by the means of density based descriptors, on the real time evolution of the excited states for the planar and twisted conformations of the DMABN (the 4-(N,N-dimethylamino)benzonitrile) molecule using Real Time-Time Dependent DFT allowed to show how the exchange-correlation functional used not only influence the energetics of the states but also their time evolution.

By employing a local (GGA, PBE), a global hybrid (PBE0) and a long range corrected (LC-PBE) functional belonging to the same family, and analyzing the results using two density based descriptors, namely the D_{CT} and the M_{AC}, our study shows that the underlying EXC modifies the evolution in time of the density.

The most evident result is that the frequency of density reorganization computed with the three functionals (PBE, PBE0 and LC-PBE) is correlated to the different percentage of Hartree-Fock exchange and thus with the delocalization of the hole and electron distributions. More specifically, the frequency of electronic interconversion of the individual determinants involved during the dynamics increases from PBE to PBE0 and to LC-PBE. Indeed, the hole-electron distance is inversely proportional to the HF exchange contribution and the greater the mean hole-electron distance during the dynamics, the lower is the frequency of density reorganization.

Supporting Information

Coordinates of the analyzed molecules, D_{CT} values during the RT simulations and Fourier transform of the MOs population for the three XC functionals.

Acknowledgements

N.R., A.P. and F.P. thank Gaussian Inc. for financial support.

N.R. and A.P. acknowledge IBiSco (Infrastructure for BIg data and Scientific COmputing) for HPC resources and the Italian Ministry of Research (projects: PRIN 202082CE3T_002) and University of Napoli Federico II (project: FRA-CosmoHab) for financial support.

References

[1] Parr G R, Yang W (1989) Density-Functional Theory of Atoms and Molecules *Oxford University Press*, USA.

[2] Runge E, Gross E K U (1984) Density-Functional Theory for Time-Dependent Systems *Phys. Rev. Lett*. 52, 997–1000.

[3] Ulrich C A (2019) Time-Dependent Density-Functional Theory: Concepts and Applications (Oxford Graduate Texts) *Oxford University Press*, USA.

[4] Grimme S, Parac M, (2003) Substantial Errors from Time-Dependent Density Functional Theory for the Calculation of Excited States of Large π Systems *ChemPhysChem* 17;4(3):292-5.

[5] Dreuw A, Weisman J L, Head-Gordon M, (2003) Long-range charge-transfer excited states in time-dependent density functional theory require non-local exchange *J. Chem. Phys. 119*, 2943.

[6] Casida, M E, Jamorski C, Casida K C, Salahub D R (1998) Molecular excitation energies to high-lying bound states from time-dependent density-functional response theory: Characterization and correction of the time-dependent local density approximation ionization threshold *J. Chem. Phys*. *108*, 4439–4449.

[7] Ottochian A, Morgillo C, Ciofini I, Frisch M J, Scalmani G, Adamo C, (2020) Double hybrids and time-dependent density functional theory: An implementation and benchmark on charge transfer excited states *J. Comput. Chem. 41*, 1242–1251.

[8] Casanova-Páez M, Goerigk L, (2020) Assessing the Tamm-Dancoff approximation, singlet-singlet, and singlet-triplet excitations with the latest long-range corrected double-hybrid density functionals *J. Chem. Phys. 153* (6), 064106.

[9] Baer R, Livshits E, Salzner U (2010) Tuned Range-Separated Hybrids in Density Functional Theory *Annu. Rev. Phys. Chem*. 61:85-109.

[10] Manna A K, Lee M H, McMahon K L, Dunietz B D (2015) Calculating High Energy Charge Transfer States Using Optimally Tuned Range-Separated Hybrid Functionals *J Chem. Theory Comput*. *11*, 1110–1117.

[11] Mardirossian N, Head-Gordon M, (2017) Thirty years of density functional theory in computational chemistry: an overview and extensive assessment of 200 density functionals *Mol. Phys. 115* (19), 2315–2372.

[12] Dreuw A, Head-Gordon M (2004) Failure of Time-Dependent Density Functional Theory for Long-Range Charge-Transfer Excited States: The Zincbacteriochlorin−Bacteriochlorin and Bacteriochlorophyll−Spheroidene Complexes *J. Am. Chem. Soc*. 126, 12, 4007–4016.

[13] Magyar R J, Tretiak S, (2007) Dependence of Spurious Charge-Transfer Excited States on Orbital Exchange in TDDFT: Large Molecules and Clusters *J. Chem. Theory Comput*. 3, 3, 976–987.

[14] Cai Z-L, Sendt K, Reimers J R (2002) Failure of density-functional theory and time-dependent density-functional theory for large extended π systems *J. Chem. Phys*. *117* 5543–5549.

[15] Tozer D J (2003) Relationship between long-range charge-transfer excitation energy error and integer discontinuity in Kohn–Sham theory *J. Chem. Phys*. *119*, 12697–12699.

[16] Slater J C (1974) The Self-Consistent Field for Molecular and Solids *Quantum Theory of Molecular and Solids, Vol. 4*, McGraw-Hill, New York.

[17] Ceperley D M, Alder B J (1980) Ground State of the Electron Gas by a Stochastic Method *Phys. Rev*. 45, 566.

[18] Perdew J P, Burke K, Ernzerhof M (1997) Generalized Gradient Approximation Made Simple *Phys. Rev. Lett*. 77, 3865.

[19] Becke A D (1988) Density-functional exchange-energy approximation with correct asymptotic behavior *Phys. Rev*. A 38, 3098.

[20] Lee C, Yang W, Parr R G (1988) Development of the Colle-Salvetti correlation-energy formula into a functional of the electron density *Phys. Rev*. B 37, 785.
[21] Adamo C, Barone V, J. (1999) Toward reliable density functional methods without adjustable parameters: The PBE0 model *Chem. Phys*. 110, 6158.
[22] Stephens P J, Devlin F J, Chabalowski C F, Frisch M J (1994) Ab Initio Calculation of Vibrational Absorption and Circular Dichroism Spectra Using Density Functional Force Fields *J. Phys. Chem.* 98:11623-11627.
[23] Yanai T, Tew D P, Handy NCA (2004) A new hybrid exchange-correlation functional using the Coulomb-attenuating method (CAM-B3LYP) *Chem. Phys. Lett.* 393: 51-57.
[24] Iikura H, Tsuneda T, Yanai T, Hirao K (2001) A long-range correction scheme for generalized-gradient-approximation exchange functionals *J. Chem. Phys.* 115:3540-3544.
[25] Casida M E. Recent Advances in Density Functional Theory, Vol. I, *World Scientific* (1995) pp 155–192.
[26] Adamo C, Jacquemin D (2013) The calculations of excited-state properties with Time-Dependent Density Functional Theory *Chem. Soc. Rev*. 42, 845-856.
[27] Calvayrac F, Reinhard P G, Suraud E (1995) Nonlinear plasmon response in highly excited metallic clusters *Phys. Rev.* 15;52(24):17056-17059.
[28] Yabana K, Bertsch G F (1996) Time-dependent local-density approximation in real time *Phys. Rev*. 15;52(24):17056-17059.
[29] Li X, Govind N, Isborn C, DePrince A E III, Lopata K (2020) Real-Time Time-Dependent Electronic Structure Theory *Chem. Rev*. 120 (18), 9951–9993.
[30]Goings J J, Lestrange P J, Li X (2018) Real-time time-dependent electronic structure theory *WIREs Comput Mol Sci* 8:e1341.
[31] Petrone A, Lingerfelt D B, Rega N, X Li (2014) From charge-transfer to a charge-separated state: a perspective from the real-time TDDFT excitonic dynamics *PCCP* 16, 24457-24465.
[32] Lopata K, Govind N (2011) Modeling Fast Electron Dynamics with Real-Time Time-Dependent Density Functional Theory: Application to Small Molecules and Chromophores *J. Chem. Theory Comput*. 7, 5, 1344–1355.
[33] Korsaye F-A, De La Lande A, Ciofini I. (2022) Following the density evolution using real time density functional theory and density based indexes: Application to model push–pull molecules *J Comput Chem.* 15;43(22):1464–73.
[34] Le Bahers T, Adamo C, Ciofini I (2011) A Qualitative Index of Spatial Extent in Charge-Transfer Excitations *J. Chem. Theory Comput*. *7*:2498–2506.
[35] Campetella M, Perfetto A, Ciofini I (2019) Quantifying partial hole-particle distance at the excited state: A revised version of the D_{CT} index *Chem. Phys. Lett*. 714, 81-86.
[36] Huet L, Perfetto A, Muniz-Miranda F, Campetella M, Adamo C, Ciofini I (2020) General Density-Based Index to Analyze Charge Transfer Phenomena: From Models to Butterfly Molecules *J. Chem.Theory Comput*. 16, 7, 4543-4553.
[37] Maschietto F, Garcia J S, Campetella M, Ciofini I (2018) Using density based indexes to characterize excited states evolution *J. Comput. Chem.* 40, 650-656.
[38] Adamo C, Le Bahers T, Savarese M, Wilbraham L, Garcıa G, Fukuda R, Ehara M, Rega N, Ciofini I (2015) Exploring excited states using Time Dependent Density Functional Theory and density based indexes *Coord. Chem. Rev. 304*, 166.
[39] Guido C A., Cortona P, Mennucci B, Adamo C (2013) On the Metric of Charge Transfer Molecular Excitations: A Simple Chemical Descriptor *J. Chem. Theory Comput. 9*, 3118.
[40] Plasser F, Wormit M, Dreuw A (2014). New tools for the systematic analysis and visualization of electronic excitations. I. Formalism *J. Chem. Phys*. *141*, 024106.
[41] Etienne T, Assfeld X, Monari A (2014) Toward a Quantitative Assessment of Electronic Transitions' Charge-Transfer Character *J. Chem. Theory Comput.* 10, 3896-3905.

[42] Plasser F (2020) TheoDORE: A toolbox for a detailed and automated analysis of electronic excited state computations *J. Chem. Phys*. 152, 084108.
[43] Peach M J G, Benfield P, Helgaker T, Tozer D J (2008) Excitation energies in density functional theory: An evaluation and a diagnostic test *J. Chem. Phys. 128*, 044118.
[44] Campetella M, Maschietto F, Frisch M J, Scalmani G, Ciofini I, Adamo C (2017) Charge transfer excitations in TDDFT: A ghost-hunter index *J. Comput. Chem.* 38(25):2151-2156.
[45] Maschietto F, Campetella M, Garcia J S, Adamo C, Ciofini I (2021) Chasing unphysical TD-DFT excited states in transition metal complexes with a simple diagnostic tool *J. Chem. Phys.* 154, 204102.
[46] Wiggins P, Williams J A G, Tozer D J. (2009) Excited state surfaces in density functional theory: A new twist on an old problem *The Journal of Chemical Physics.* 7;131(9):091101.
[47] Rappoport D, Furche F. (2004) Photoinduced Intramolecular Charge Transfer in 4-(Dimethyl)aminobenzonitrile − A Theoretical Perspective *J Am Chem Soc.* 1;126(4):1277–84.
[48] Georgieva I, Aquino A J A, Plasser F, Trendafilova N, Köhn A, Lischka H. (2015) Intramolecular Charge Transfer Excited-State Processes in 4-(N, N -Dimethylamino)benzonitrile: The Role of Twisting and the $\pi\sigma^*$ State *J Phys Chem A.* 18;119(24):6232–43.
[49] Kochman M A, Tajti A, Morrison C A, Miller R J D. (2015) Events in the Nonadiabatic Relaxation Dynamics of 4-(N,NDimethylamino)benzonitrile *J Chem Theory Comput.* 10;11(3):1118–28.
[50] Curchod BFE, Sisto A, Martínez TJ. (2017) Ab Initio Multiple Spawning Photochemical Dynamics of DMABN Using GPUs *J Phys Chem A.* 12;121(1):265–76.
[51] Cogan S, Zilberg S, Haas Y. (2006) The Electronic Origin of the Dual Fluorescence in Donor-Acceptor Substituted Benzene Derivatives *J Am Chem Soc.* 1;128(10):3335–45.
[52] Gómez I, Reguero M, Boggio-Pasqua M, Robb M A (2005) Intramolecular Charge Transfer in 4-Aminobenzonitriles Does Not Necessarily Need the Twist *J Am Chem Soc.* 1;127(19):7119–29.
[53] Rotkiewicz K, Grellmann K H, Grabowski Z R (1973) Reinterpretation of the anomalous fluorescense of p-n,n-dimethylamino-benzonitrile *Chemical Physics Letters.*;19(3):315–8.
[54] Zachariasse K A, Grobys M, Von Der Haar Th, Hebecker A, Il'ichev YuV, Morawski O, Rückert I, Kühnle W (1997) Photo-induced intramolecular charge transfer and internal conversion in molecules with a small energy gap between S_1 and S_2. Dynamics and structure *Journal of Photochemistry and Photobiology A: Chemistry.* 105(2–3):373–83.
[55] Sobolewski A L, Domcke W (1996) Charge transfer in aminobenzonitriles: Do they twist? *Chemical Physics Letters.* 250(3–4):428–36.
[56] Coto P B, Serrano-Andrés L, Gustavsson T, Fujiwara T, Lim E C (2011) Intramolecular charge transfer and dual fluorescence of 4-(dimethylamino)benzonitrile: ultrafast branching followed by a two-fold decay mechanism *Phys Chem Chem Phys.* 13(33):15182.
[57] Köhn A, Hättig C. (2004) On the Nature of the Low-Lying Singlet States of 4-(Dimethyl-amino)benzonitrile *J Am Chem Soc.* 126(23):7399–410.
[58] Goings J J, Lestrange P J, Li X (2018) Real-time time-dependent electronic structure theory *WIREs Computational Molecular Science* 8 (1), e1341.
[59] Petrone A, Lingerfelt D B, Rega N, Li X (2014) From charge-transfer to a charge-separated state: a perspective from the real-time TDDFT excitonic dynamics *Physical Chemistry Chemical Physics* 16 (44), 24457–24465.
[60] Kasper J M, Lestrange P J, Stetina T F, Li X (2018) Modeling $L_{2,3}$-Edge X-ray Absorption Spectroscopy with Real-Time Exact Two-Component Relativistic Time-Dependent Density Functional Theory *J Chem Theory Comput* 14 (4), 1998–2006.
[61] Peng B, Lingerfelt D B, Ding F, Aikens C M, Li X (2015) Real-time TDDFT studies of exciton decay and transfer in silver nanowire arrays *Journal of Physical Chemistry C* 119 (11), 6421–6427.
[62] Donati G, Lingerfelt D B, Aikens C M, Li X (2018) Anisotropic polarizability-induced plasmon transfer *Journal of Physical Chemistry C* 122 (19), 10621–10626.

[63] Perrella F, Petrone A, Rega N (2023) Understanding Charge Dynamics in Dense Electronic Manifolds in Complex Environments *J Chem Theory Comput* 19 (2), 626–639.
[64] Perrella F, Li X, Petrone A, Rega N (2023) Nature of the Ultrafast Interligands Electron Transfers in Dye-Sensitized Solar Cells *JACS* 3 (1), 70–79.
[65] Frensley W R (1990) Boundary conditions for open quantum systems driven far from equilibrium *Rev Mod Phys* 62 (3), 745.
[66] Li X, Smith S M, Markevitch A N, Romanov D A, Levis R J, Schlegel H B (2005) A time-dependent Hartree–Fock approach for studying the electronic optical response of molecules in intense fields *Physical Chemistry Chemical Physics* 7 (2), 233–239.
[67] Frisch, M. J.; Trucks, G. W.; Schlegel, H. B.; Scuseria, G. E.; Robb, M. A.; Cheeseman, J. R.; Scalmani, G.; Barone, V.; Petersson, G. A.; Nakatsuji, H.; Li, X.; Caricato, M.; Marenich, A. V.; Bloino, J.; Janesko, B. G.; Gomperts, R.; Mennucci, B.; Hratchian, H. P.; Ortiz, J. V.; Izmaylov, A. F.; Sonnenberg, J. L.; Williams-Young, D.; Ding, F.; Lipparini, F.; Egidi, F.; Goings, J.; Peng, B.; Petrone, A.; Henderson, T.; Ranasinghe, D.; Zakrzewski, V. G.; Gao, J.; Rega, N.; Zheng, G.; Liang, W.; Hada, M.; Ehara, M.; Toyota, K.; Fukuda, R.; Hasegawa, J.; Ishida, M.; Nakajima, T.; Honda, Y.; Kitao, O.; Nakai, H.; Vreven, T.; Throssell, K.; Montgomery, J. A., Jr.; Peralta, J. E.; Ogliaro, F.; Bearpark, M. J.; Heyd, J. J.; Brothers, E. N.; Kudin, K. N.; Staroverov, V. N.; Keith, T. A.; Kobayashi, R.; Normand, J.; Raghavachari, K.; Rendell, A. P.; Burant, J. C.; Iyengar, S. S.; Tomasi, J.; Cossi, M.; Millam, J. M.; Klene, M.; Adamo, C.; Cammi, R.; Ochterski, J. W.; Martin, R. L.; Morokuma, K.; Farkas, O.; Foresman, J. B.; Fox, D. J. *Gaussian 16, Revision C.01*; Gaussian, Inc., Wallingford CT, 2016.
[68] Frisch, M. J.; Trucks, G. W.; Schlegel, H. B.; Scuseria, G. E.; Robb, M. A.; Cheeseman, J. R.; Scalmani, G.; Barone, V.; Petersson, G. A.; Nakatsuji, H.; Li, X.; Caricato, M.; Marenich, A. V.; Bloino, J.; Janesko, B. G.; Gomperts, R.; Mennucci, B.; Hratchian, H. P.; Ortiz, J. V.; Izmaylov, A. F.; Sonnenberg, J. L.; Williams-Young, D.; Ding, F.; Lipparini, F.; Egidi, F.; Goings, J.; Peng, B.; Petrone, A.; Henderson, T.; Ranasinghe, D.; Zakrzewski, V. G.; Gao, J.; Rega, N.; Zheng, G.; Liang, W.; Hada, M.; Ehara, M.; Toyota, K.; Fukuda, R.; Hasegawa, J.; Ishida, M.; Nakajima, T.; Honda, Y.; Kitao, O.; Nakai, H.; Vreven, T.; Throssell, K.; Montgomery, J. A., Jr.; Peralta, J. E.; Ogliaro, F.; Bearpark, M. J.; Heyd, J. J.; Brothers, E. N.; Kudin, K. N.; Staroverov, V. N.; Keith, T. A.; Kobayashi, R.; Normand, J.; Raghavachari, K.; Rendell, A. P.; Burant, J. C.; Iyengar, S. S.; Tomasi, J.; Cossi, M.; Millam, J. M.; Klene, M.; Adamo, C.; Cammi, R.; Ochterski, J. W.; Martin, R. L.; Morokuma, K.; Farkas, O.; Foresman, J. B.; Fox, D. J. *Gaussian Development Version Revision J.01*; Gaussian, Inc., Wallingford, CT, 2018.

TOC Graphic